Available online at www.sciencedirect.com
ScienceDirect
Journal of Asian Earth Sciences 29 (2007) 737–750
Journal of Asian Earth Sciences
www.elsevier.com/locate/jaes

Geochemistry of Cretaceous granites from Mianning in the Panxi region, Sichuan Province, southwestern China: Implications for their generation

Cheng Xu [a,*], Zhilong Huang [a], Liang Qi [b], Pingqing Fu [a], Congqiang Liu [a], Endong Li [a], Tao Guan [a]

[a] *Institute of Geochemistry, Chinese Academy of Sciences, Guiyang 550002, China*
[b] *Department of Earth Sciences, University of Hong Kong, Hong Kong, China*

Received 16 April 2004; received in revised form 14 October 2005; accepted 8 March 2006

Abstract

The Cretaceous granites of Mianning, located in the northern Panxi region, were emplaced after collision of the Tibetan Plateau and Yangtze Block. These granites have very high $K_2O + Na_2O$, Ga, Zr, Nb, Y, REE (except Eu), and very low MgO, CaO, P_2O_5, and Sr contents relative to M-, I- or S-type granites. Based on the chemical discrimination criteria of Whalen et al . [Whalen, J.B., Currie, K.L., Chappell, B.W., 1987. A-type granites: geochemical characteristics, distribution and petrogenesis. Contributions to Mineralogy and Petrology 95, 407–419], most of them are A-type granites. Moreover, the granites plot in the range of post-collision granites and belong to the A2 type. Elevated initial Sr isotopic ratios (>0.72) suggest their derivation dominantly from a crustal source. These features are consistent with granite formation in a post-orogenic setting, such as after subduction or collision between of the Tibetan Plateau and Yangtze Block. In addition, the granites are characterized by low abundances of Ba, Sr, P, Ti, and Eu, positive correlation between Ba and Eu anomalies, and negative correlation between Rb and K/Rb. Plots of Rb vs. Sr suggest that fractional crystallization affected the final compositions of these granites after melting from a dominantly crustal source. From the late Proterozoic to late Mesozoic, the crustal composition, compared to that of the mantle, appears to have increased in the Panxi region. While the mantle component played an important part in the generation of Cretaceous granites in southeastern China, its influence was relatively minor in the Panxi region. Thus, there was a significant difference in mantle evolution between southeastern China and the Panxi region, which led to different metallogenic processes.

Keywords: Cretaceous granites; Geochemistry; A-type; Crustal source; Panxi region

1. Introduction

The Panxi region is an important mineralization belt of metals and nonmetals in China, including tungsten, tin, molybdenum, beryllium, iron, nickel, titanium, rare earth elements, niobium, tantalum, uranium, thorium, and phosphorus. Large volumes of granite occur in the region. The granites formed in three episodes (Liu et al., 1988; Zhang et al., 1988; Niu, 1994; Zhou et al., 2002), i.e., (1) late Proterozoic in Mopanshan (biotite K–Ar age of 808 Ma), Mosaying (biotite K–Ar age of 700–800 Ma) and Miyi (SHRIMP U–Pb zircon age of 764 ± 9 Ma); (2) late Permian to Triassic in Taihe, Cida (whole-rock Rb–Sr age of 230 Ma), Dukou and Hongge (biotite K–Ar age of 256–262 Ma); and (3) Cretaceous (whole-rock and biotite K–Ar ages of 110–132 Ma, 78–134 Ma, respectively), represented by the Mianning granites in the northern margin of the Panxi region (Fig. 1). Prior studies showed that the late Proterozoic Mopanshan and Mosaying granites are I- and S-type, respectively, and that the late Permian to Triassic Taihe and Cida granites are A-type that were emplaced in a rift setting (Liu et al., 1988; Zhang et al.,

* Corresponding author.
E-mail address: xucheng1999@hotmail.com (C. Xu).

1367-9120/$ - see front matter © 2006 Elsevier Ltd. All rights reserved.
doi:10.1016/j.jseaes.2006.03.013

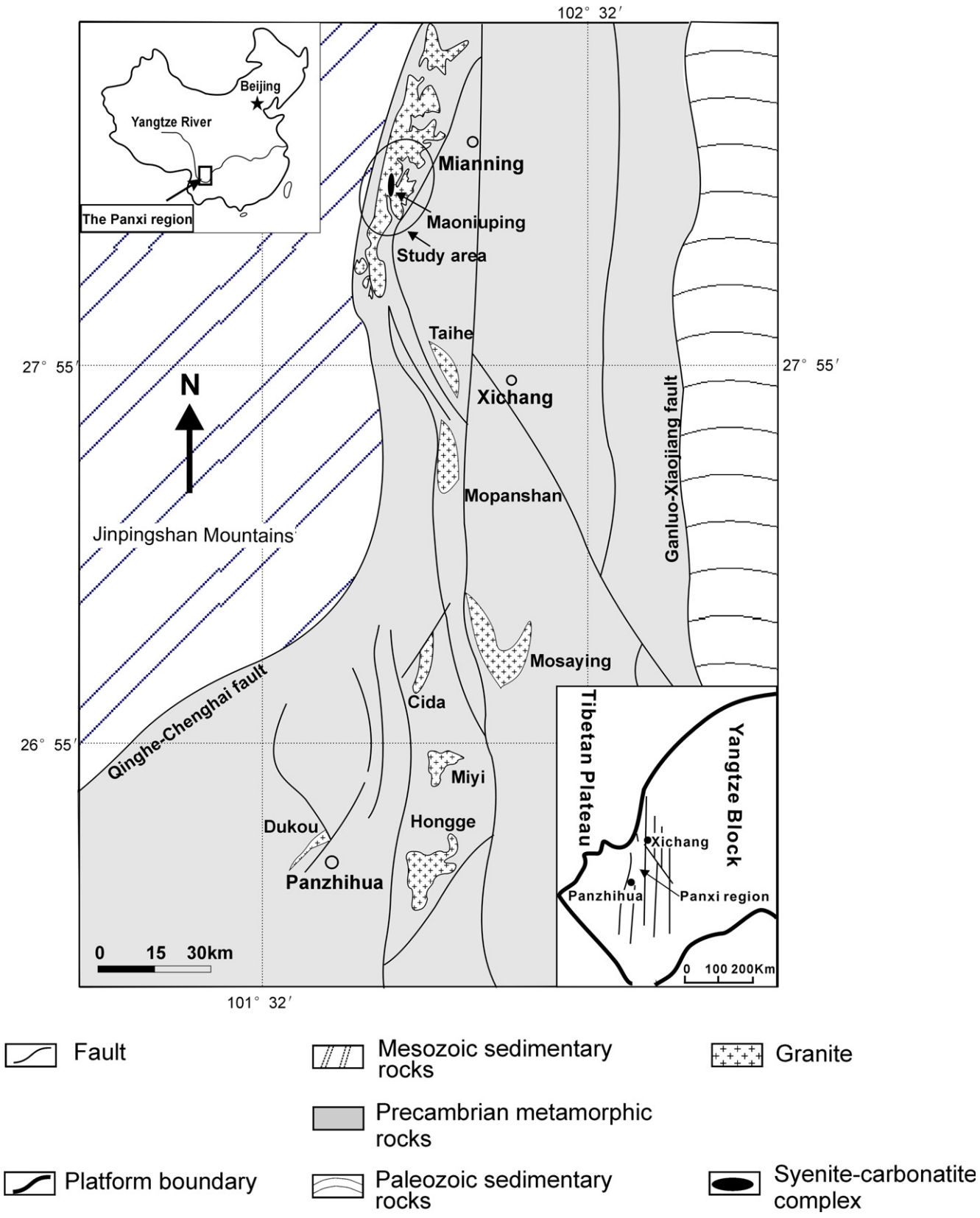

Fig. 1. Geologic map of granites in the Panxi region (modified after Liu et al., 1988; Zhang et al., 1988).

1988). Due to the difficult access to the northern part of the Panxi region, little geochemical study has been carried out on the Cretaceous granites. Consequently, the origin of the Cretaceous granites is not well understood. Most metallogenic processes in southeastern China took place in the late Mesozoic (Hua and Mao, 1999; Mao and Hua, 1999),

whereas mineralization in the Panxi region and West China was minimal during the some time interval. A number of deposits in the Panxi region formed in the early Paleozoic to early Mesozoic, and Cenozoic (Zhang et al., 1988; Xu et al., 2003a). In this paper, we present new geochemical and Sr–Nd isotopic data for Cretaceous granites and rhyolites. In addition, we discuss their petrogenesis, tectonic setting for magma generation and general implications for metallogenesis in the Panxi region.

2. Geological setting and sampling

The Panxi region is situated between the Panzhihua and Xichang areas in Sichuan Province, southwestern China. It is tectonically located in the western margin of the Yangtze Block, next to the Tibetan Plateau. The eastern and western sides are bordered by the Ganluo-Xiaojiang and Qinghe-Chenghai faults, respectively (Fig. 1). The crystalline basement of the region consists mostly of the Neoproterozoic moderate to high-grade metamorphic Kangding complex, a spilite-keratophyre sequence with greenschist facies metamorphism and an epimetamorphic sedimentary rock sequence (Cong, 1988; Zhou et al., 2002). Overlying the crystalline basement is the Neoproterozoic to Cenozoic neritic sequence with carbonate facies. Silurian, Devonian and Carboniferous units are not present in this area due to erosion of the region during an early stage of rifting.

Outcrops typically consist of layered plutonic sequences and an alkalic ring complex. In the axial part of the region, voluminous basalt, syenite, and granite were emplaced. The Cretaceous Mianning granite, located in the northern margin of the Panxi region, covers an area of about 700 km^2 with a length of 80 km. A Himalayan alkalic syenite and carbonatite complex (whole-rock K–Ar ages of 28–48 Ma and 31.7 ± 0.7 Ma, respectively; Pu, 2001) intruded the center of the Cretaceous granites. Minor rhyolites also occur. The study area is confined to the central part of the Mianning granites (Fig. 1).

The studied granites are easily grouped by color (red and gray) and grain size. They include a red, medium-grained granite (RMG), a gray, medium- to fine-grained granite (GMG), and a gray, fine-grained granite (GFG). Red granites are characterized by prophyritic and massive texture. In GMG and GFG, graphic texture is common and the rocks are composed of K-feldspar, albite and quartz, with minor amounts of biotite, sericite, and accessory minerals such as apatite, zircon, monazite, allanite, titanite, and magnetite. Occasionally, aegirine and small amounts of hematite and pyrite are found in GFG. Some of the quartz display allotriomorphic-granular textures with growth along cleavages.

3. Analytical methods

The major elements of whole-rock samples were determined by wet chemical methods at the Institute of Geochemistry, Chinese Academy of Sciences. Trace elements (REE included) were analyzed in solution by ICP-MS at the Institute of Geochemistry, Chinese Academy of Sciences. Details are given in Qi et al. (2000). Fifty milligrams of whole-rock powder were dissolved in a Teflon bomb using 1 ml HF (38%) and 0.5 ml HNO_3 (68%). The sealed bomb was placed in an electric oven and heated to 190 °C for 12 h. One milliliter of 1 $\mu g\,ml^{-1}$ Rh was added to the cooled solution as the internal standard and the solution was then evaporated. One milliliter of HNO_3 (68%) was added, evaporated to dryness and followed by a second addition of HNO_3 and evaporation to dryness. The final residue was re-dissolved in 8 ml HNO_3 (40%). The bomb was sealed and heated in an electric oven at 110 °C for 3 h. The final solution was diluted to 100 ml by addition of distilled de-ionized water for ICP-MS analysis. The analytical precision for most elements is generally better than 10%.

Sr and Nd isotopic compositions were analyzed at the Institute of Geochemistry and the Institute of Geology and Geophysics of the Chinese Academy of Sciences. The analytical procedures for both Sr and Nd isotopic determinations were similar. Samples were dissolved in $HF + HClO_4$. Rb, Sr, and REE were separated using AGW50 × 12 cation exchange columns. The REE were further dissolved in 0.1 N HCl, then Sm and Nd were separated on the levextrel resin ion exchange columns. $^{87}Rb/^{86}Sr$ and $^{147}Sm/^{144}Nd$ ratios analyzed at the Institute of Geochemistry were calculated using the Rb, Sr, Sm, and Nd abundances measured by ICP-MS. Several analyses on the NBS-987 Sr standard yielded $^{87}Sr/^{86}Sr = 0.710254 \pm 5$ at the Institute of Geochemistry. The mean $^{143}Nd/^{144}Nd$ ratios in the La Jolla and Jndi-1 Nd standard were 0.511838 ± 8 at the Institute of Geology and Geophysics, 0.512078 ± 7 at the Institute of Geochemistry, respectively. $^{143}Nd/^{144}Nd$ ratios were normalized to the value of $^{146}Nd/^{144}Nd = 0.7219$. Fractionation effects during the Sr isotopic composition runs were eliminated by normalizing to a $^{86}Sr/^{88}Sr$ value of 0.1194.

4. Geochemistry

4.1. Element geochemistry

The results of major, trace and rare earth element analyses for granite and rhyolite samples are given in Table 1.

The granites are typical in their major element concentrations ($SiO_2 = 67$–75%, $TiO_2 = 0.12$–0.72%, $Fe_2O_3 = 0.82$–1.74%, $MnO = 0.01$–0.07%, $MgO = 0.20$–0.80%, $CaO = 0.20$–0.85%, $P_2O_5 = <0.01$–0.12%), but are alkalic, with $K_2O = 3.7$–6.3% and $Na_2O = 2.2$–7.0%. They appear fractionated in that $Fe_2O_3 > MgO$.

The primitive-mantle-normalized spidergrams of the granites are similar (Fig. 2). Chondrite-normalized REE patterns for the granites are uniform (except for sample MX-87; Fig. 3). They show negative Eu anomalies (0.16–0.39 for RMG; 0.34–0.57 for GMG; 0.14–0.39 for GFG), moderate light REE enrichment ($La/Nd_N =$

Table 1
Major (wt%) and trace (ppm) element compositions of granites and rhyolites from Mianning in the Panxi region

Sample no.:	MNP-32	MX-46	MNP-50	MX-53	MX-59	MX-61	MNP-73	MX-25	MX-27	MNP-44	MX-56	MNP-60	MNP-78	MNP-30	MX-34	MX-36	MX-55	MX-58	MX-63	MX-68	MX-87	MNP-31	MNP-89	MX-92	MNP-135
Type:	RMG	RMG	RMG	RMG	RMG	RMG	RMG	GMG	GMG	GMG	GMG	GMG	GMG	GFG	GFG	GFG	GFG	GFG	GFG	GFG	GFG	Rh	Rh	Rh	Rh
SiO_2	73.45	75.01	74.46	71.27	71.55	72.32	73.23	69.76	70.53	71.95	71.03	71.92	73.27	73.56	73.98	72.07	72.89	74.82	73.98	73.55	67.01	74.99	77.93	72.89	78.96
TiO_2	0.37	0.72	0.32	0.17	0.42	0.14	0.36	0.14	0.25	0.30	0.47	0.31	0.55	0.62	0.55	0.12	0.15	0.23	0.13	0.35	0.13	0.14	<0.01	<0.01	<0.01
Al_2O_3	12.82	12.33	13.09	14.00	14.03	13.56	11.89	14.96	13.93	12.93	13.56	13.56	11.99	12.69	13.56	13.96	13.77	11.69	13.50	12.39	18.00	12.93	10.52	13.56	11.76
Fe_2O_3	1.38	1.28	1.23	1.59	1.14	1.28	1.33	1.61	1.57	1.74	1.58	1.49	1.30	0.93	1.25	1.32	0.82	1.17	1.13	1.44	1.11	1.10	1.00	0.84	0.79
FeO	1.02	1.00	0.70	1.50	1.00	1.20	1.02	1.55	1.34	1.23	1.23	1.34	1.63	1.00	0.90	0.89	0.40	0.65	1.11	0.90	0.29	0.95	0.51	0.40	0.20
MnO	0.03	0.02	0.03	0.03	0.02	0.03	0.03	0.02	0.04	0.03	0.03	0.03	0.04	0.03	0.02	0.03	0.03	0.01	0.02	0.04	0.07	0.02	0.02	0.01	<0.01
MgO	0.20	0.20	0.40	0.49	0.20	0.50	0.40	0.60	0.30	0.30	0.60	0.60	0.80	0.30	0.60	0.23	0.36	0.30	0.53	0.40	0.33	0.32	0.40	0.80	0.60
CaO	0.70	0.20	0.30	0.70	0.30	0.30	0.70	0.40	0.70	0.80	0.60	0.40	0.60	0.30	0.20	0.52	0.85	0.30	0.50	0.50	0.67	0.30	0.30	0.20	0.10
Na_2O	3.64	3.61	3.64	4.46	3.60	3.70	3.79	3.97	3.83	4.01	3.97	3.85	4.01	3.49	2.29	3.82	3.59	3.38	2.16	3.73	7.02	3.83	2.74	4.28	1.50
K_2O	4.60	4.44	4.80	5.24	5.11	5.14	4.93	4.55	4.80	4.35	5.13	4.98	3.72	4.83	4.25	6.25	5.68	4.58	5.60	5.39	4.15	3.62	4.25	5.42	3.46
P_2O_5	<0.01	<0.01	<0.01	0.08	<0.01	<0.01	<0.01	<0.01	<0.01	<0.01	<0.01	<0.01	<0.01	<0.01	<0.01	0.08	0.07	<0.01	0.07	<0.01	0.12	<0.01	<0.01	<0.01	<0.01
H_2O	1.08	1.09	0.73	0.62	2.39	0.95	1.53	1.72	1.94	1.50	1.70	1.02	1.22	1.69	1.65	0.80	1.22	2.37	1.07	1.22	0.92	0.97	1.45	0.73	1.77
Total	99.29	99.90	99.70	100.15	99.76	99.12	99.21	99.28	99.13	99.14	99.90	99.50	99.13	99.44	99.25	100.09	99.83	99.50	99.80	99.91	99.82	99.17	99.12	99.13	99.10
Sr	39.3	23.0	47.5	29.3	35.6	34.7	44.1	29.9	54.3	55.8	30.1	34.8	104	34.9	34.5	11.2	42.6	30.5	36.1	40.6	34.7		39.1	144	14.4
Rb	189	172	243	197	229	209	179	185	190	186	208	202	139	233	235	234	248	221	227	180	177		177	272	133
Ba	476	393	657	616	383	696	624	548	633	590	515	542	917	337	548	293	808	311	678	639	709		459	3846	593
Th	22.2	21.2	33.1	20.7	29.0	20.8	22.9	22.8	21.0	21.3	22.2	22.1	11.2	27.3	14.7	27.1	34.2	25.9	15.0	27.0	97.9		14.2	14.8	13.4
Ta	1.26	1.54	3.13	1.14	2.13	1.15	1.38	1.21	1.13	1.09	1.18	1.27	0.541	2.46	0.765	1.88	2.46	2.68	0.751	1.5	1.03		0.713	0.601	0.971
Nb	15.4	19.4	45.8	12.9	23.3	12.4	15.6	15.4	14.0	13.7	14.6	15.2	5.43	31.7	7.17	22.8	39.5	29.7	7.25	17.1	38.2		0.547	0.324	1.30
Hf	8.84	10.0	11.4	6.40	10.1	8.97	9.28	9.37	8.06	9.07	9.91	9.94	5.04	10.1	4.59	8.46	10.2	9.35	4.58	10.3	8.32		3.79	4.92	7.02
Zr	255	271	279	188	245	265	258	255	271	279	245	265	258	260	117	210	288	210	140	294	332		39.1	144	14.4
Y	28.8	56.0	89.4	33.0	60.2	35.8	37.3	36.3	34.7	33.7	38.2	36.6	25.2	72.8	21.0	50.1	31.6	73.2	25.7	11.8	21.7		24.1	29.3	26.5
Yb	3.30	6.06	10.4	3.27	6.96	4.08	4.05	3.96	3.49	3.66	3.89	4.12	2.72	7.72	2.49	6.01	3.28	8.44	2.84	1.26	1.43		3.26	3.23	3.57
Sc	4.33	4.11	3.71	3.75	3.51	4.37	4.48	5.28	4.60	4.24	5.09	5.16	5.60	3.47	4.64	1.04	2.90	2.53	3.32	4.22	2.35		2.80	2.85	3.03
Ni	2.60	2.90	3.24	4.64	2.54	5.90	2.78	3.74	3.46	3.61	3.69	7.54	7.95	2.14	3.57	2.21	5.19	3.61	6.62	3.84	5.39		2.67	2.16	1.50
Cu	11.6	20.0	24.3	30.3	15.1	29.7	19.4	23.6	27.3	19.4	21.5	19.3	26.0	25.0	19.6	25.7	26.7	6.73	37.6	12.3	34.4		4.64	13.8	7.64
Ga	18.4	18.1	25.1	17.1	25.8	18.4	18.2	18.8	18.3	18.2	19.7	19.7	17.2	23.2	19.6	18.4	22.7	22.6	18.5	19.0	30.2		14.2	25.0	21.4
La		45.6		42.7	61.9	38.1		43.2	40.6		43.7		35.6	56.8	29.1	27.7	40.5	52.3	30.6	18.8	56.4			63.3	
Ce		102		77.1	140	76.5		83.4	81.3		87.1		59.0	118	50.2	104	53.5	103	51.8	29.8	88.3			119	
Pr		10.7		8.33	14.6	7.85		8.74	8.19		8.87		6.72	13.2	5.50	6.54	5.86	11.2	5.87	3.22	9.69			15.9	
Nd		38.9		28.7	51.7	25.9		29.8	27.6		30.4		22.4	46.6	19.2	23.8	17.3	40.3	20.6	11.0	30.1			49.1	
Sm		7.93		5.25	11.0	5.18		5.81	5.33		6.10		4.64	9.86	3.48	4.84	2.20	8.63	3.93	2.20	3.40			7.36	
Eu		0.62		0.599	0.559	0.652		0.627	0.62		0.692		0.801	0.549	0.389	0.337	0.506	0.438	0.414	0.208	0.78			0.905	
Gd		7.79		5.53	9.98	5.09		5.43	4.93		5.67		3.99	9.95	3.74	6.21	8.36	10.6	4.27	2.14	11.2			5.68	
Tb		1.55		0.856	1.66	0.927		0.955	0.919		1.02		0.676	1.82	0.561	1.10	0.965	1.82	0.638	0.304	1.15			0.922	

Dy	9.10	5.34	9.87	5.56	5.81	5.67	6.12	4.5	11.6	3.34	8.07	4.91	12.2	4.04	1.76	4.29		5.13
Ho	1.97	1.08	1.99	1.17	1.21	1.13	1.24	0.942	2.47	0.729	1.88	0.99	2.66	0.88	0.40	0.75		1.01
Er	5.48	3.23	5.81	3.51	3.37	3.20	3.69	2.54	7.13	2.24	5.58	2.92	8.24	2.47	1.13	1.86		2.83
Tm	0.867	0.508	1.02	0.546	0.533	0.499	0.585	0.381	1.16	0.35	0.889	0.453	1.23	0.441	0.172	0.259		0.472
Yb	6.06	3.27	6.96	4.08	3.96	3.49	3.89	2.72	7.72	2.49	6.01	3.28	8.44	2.84	1.26	1.43		3.23
Lu	0.828	0.465	0.988	0.569	0.545	0.509	0.561	0.432	1.12	0.394	0.909	0.522	1.18	0.437	0.195	0.226		0.502
∑REE	239.4	183.0	318.0	175.6	193.3	184.0	199.6	145.3	288.0	121.7	198.0	142.3	262.2	129.2	72.6	209.9		275.3
δCe	1.11	0.98	1.12	1.07	1.03	1.07	1.06	0.92	1.04	0.95	1.86	0.84	1.02	0.93	0.92	0.91		0.91
δEu	0.24	0.34	0.16	0.39	0.34	0.37	0.36	0.57	0.17	0.33	0.19	0.36	0.14	0.31	0.29	0.39		0.43
La/Yb_N	5.08	8.82	6.0	6.28	7.35	7.85	7.58	8.81	4.96	7.89	3.11	8.31	4.18	7.27	10.1	26.6		13.2
La/Nd_N	2.27	2.0	2.32	2.85	2.80	2.85	2.78	3.07	2.36	2.94	2.26	4.52	2.52	2.88	3.33	3.63		2.50
Gd/Yb_N	1.04	1.37	1.16	1.01	1.11	1.14	1.18	1.18	1.04	1.21	0.83	2.05	1.02	1.22	1.37	6.31		1.42

RMG, red medium-grained granite; GMG, gray medium- to fine-grained granite; GFG, gray fine-grained granite; Rh, rhyolite.

2.0–2.85, 2.78–3.07, 2.26–4.52 for RMG, GMG, GFG, respectively), and nearly flat heavy REE distributions ($Gd/Yb_N = 1.01–1.37$, 1.11–1.18, 0.83–1.37 for RMG, GMG, GFG, respectively).

The RMG, GMG, and GFG all show similar major and trace element geochemistry except that the GFG displays variable REE patterns. Two rhyolites have slightly higher SiO_2, and lower TiO_2, FeO, Nb, and Zr contents than the granites. Moreover, they are characterized by lower CaO and P_2O_5. In the spidergram, the rhyolites show characteristic negative anomalies in Ba (one exception), Nb, P_2O_5, and TiO_2 (Fig. 2D). Sample Mx-92 also displays a negative Eu anomaly, moderate light REE enrichment and nearly flat heavy REE distribution (Fig. 3D). Whether the rhyolites and granites are contemporaneous and evolved from the same source, however, is difficult to answer and will require more evidence.

4.2. Isotope geochemistry

Sr–Nd isotopic data are presented in Table 2 and plotted in Fig. 4. Initial $^{87}Sr/^{86}Sr$ and $^{143}Nd/^{144}Nd$ ratios were calculated assuming an emplacement age of 120 Ma. However, the granites have a small range of moderately negative ε_{Nd} values (−3.2 to −1.5), while initial $^{87}Sr/^{86}Sr$ ratios are very high (>0.72) and variable. This indicates that the crustal component played an important role in the generation of the Cretaceous granites, although part of the mantle material was possibly involved because of the moderately negative ε_{Nd} values. Similar high and variable initial $^{87}Sr/^{86}Sr$ values were also found in north Himalayan leucogranites with $(^{87}Sr/^{86}Sr)_0$ values of 0.7344–0.8505 (Zhang et al., 2005). This characteristic is shared by other Himalayan granites and migmatites (Inger and Harris, 1993). Inger and Harris (1993) suggested that the highly peraluminous, low-calcium, high initial $^{87}Sr/^{86}Sr$ compositions of the Himalayan leucogranites were indicative of magmas derived from crustal melting. Typically, they do not define an isochron because of the heterogeneous crustal sources and incomplete mixing of magma batches (Deniel et al., 1987).

5. Discussion

5.1. Classification

In a plot of A/NK vs. A/CNK (A/CNK= molar ratios of $Al_2O_3/(CaO + K_2O + Na_2O)$) (Maniar and Piccoli, 1989), these rocks are peraluminous to slightly metaluminous (Fig. 5). Their geochemical characteristics are distinguished from M-, S-, and I-type granites (Whalen et al., 1987), but are similar to A-type granites (Fig. 6). Although the Fe/Mg and $10{,}000 \times Ga/Al$ ratios, LREE, Y, Nb, and Zr contents in these granites are lower than the global average for A-type granites (Whalen et al., 1987), Anderson and Morrison (1992) have shown that peraluminous A-type granites characteristically have lower levels of Fe/Mg ratios. The low $10{,}000 \times Ga/Al$ ratios for peraluminous

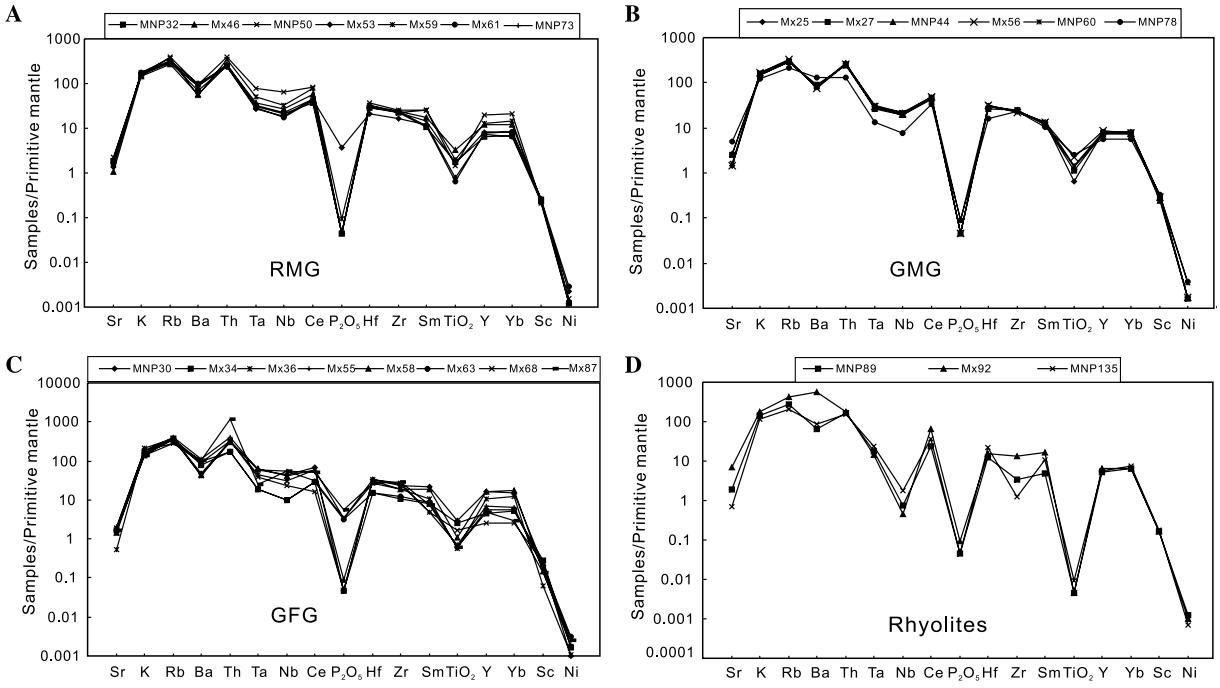

Fig. 2. Primitive-mantle-normalized spidergrams for (A) RMG (red medium-grained granite), (B) GMG (gray medium- to fine-grained granite), (C) GFG (gray fine-grained granite), (D) rhyolite. The primitive-mantle values are from Sun and McDonough (1989). Ce and Nd contents of sample MNP are from Xu et al. (2003a).

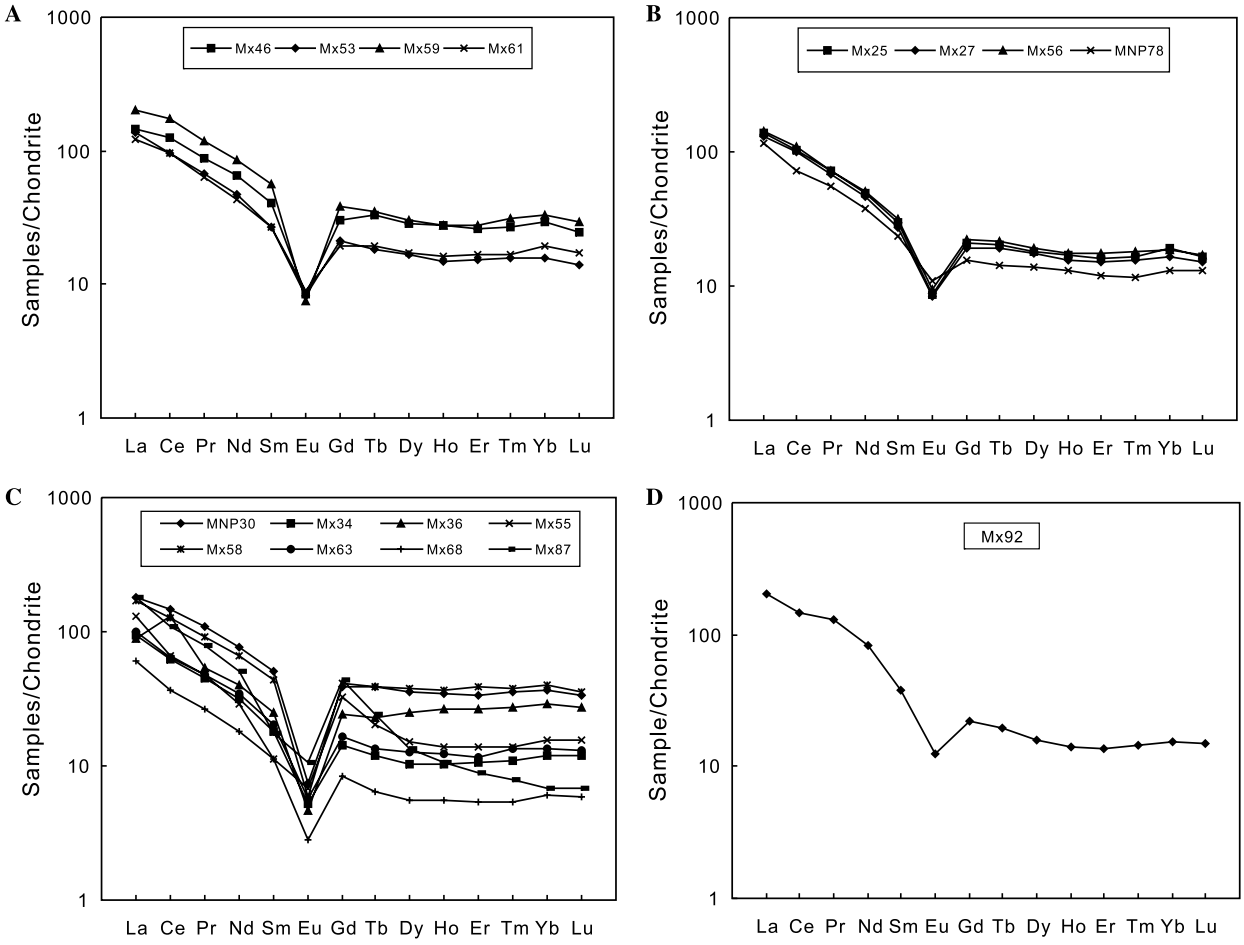

Fig. 3. Chondrite-normalized REE patterns for (A) red medium-grained granite, (B) gray medium- to fine-grained granite, (C) gray fine-grained granite, (D) rhyolite. The data of Boynton (1984) were used for normalization.

Table 2
Sr and Nd isotopic compositions of granites from Mianning in the Panxi region

Sample:	MX-36	MNP-42[a]	MNP-50[a]	MX-53	MX-56	MX-58	MNP-78[a]	MX-87
Type:	GFG	RMG	RMG	RMG	GMG	GFG	GMG	GFG
$^{147}Sm/^{144}Nd$	0.1229	0.0619	0.1241	0.1106	0.1213	0.1232	0.1161	0.0683
$^{143}Nd/^{144}Nd \pm (2se)$	0.512503 ± 15	0.512419 ± 10	0.512444 ± 12	0.512448 ± 16	0.512417 ± 19	0.512458 ± 13	0.512494 ± 11	0.512450 ± 9
$(^{143}Nd/^{144}Nd)_0$	0.51241	0.51237	0.51235	0.51236	0.51232	0.51236	0.51240	0.51240
ε_{Nd} (T)	−1.5	−2.2	−2.7	−2.4	−3.2	−2.4	−1.6	−1.7
DM model age (Ma)	910	630	1010	880	1030	980	860	630
$^{87}Rb/^{86}Sr$	59.65	10.64	18.84	19.20	19.86	21.87	4.974	14.58
$^{87}Sr/^{86}Sr \pm (2se)$	0.822642 ± 10	0.743765 ± 10	0.819719 ± 13	0.822642 ± 11	0.889401 ± 12	0.878174 ± 12	0.744440 ± 12	0.835757 ± 10
$(^{87}Sr/^{86}Sr)_0$	0.7209	0.7257	0.7876	0.7899	0.8555	0.8409	0.7360	0.8109

[a] Xu et al. (2003a). Samples MNP-42, 50, 78, and MX-58 were analyzed at the Institute of Geology and Geophysics. The other samples were analyzed at the Institute of Geochemistry. DM model age is calculated using the equation of DePaolo (1981), $\varepsilon_{Nd}(T) = 0.25T^2 - 3T + 8.5$. Abbreviations as in Table 1.

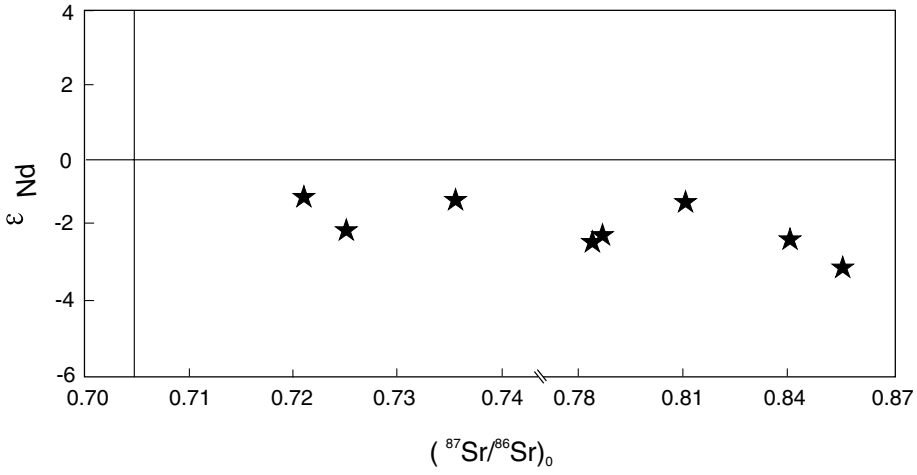

Fig. 4. ε_{Nd} vs. initial $^{87}Sr/^{86}Sr$ diagram. (★) granite.

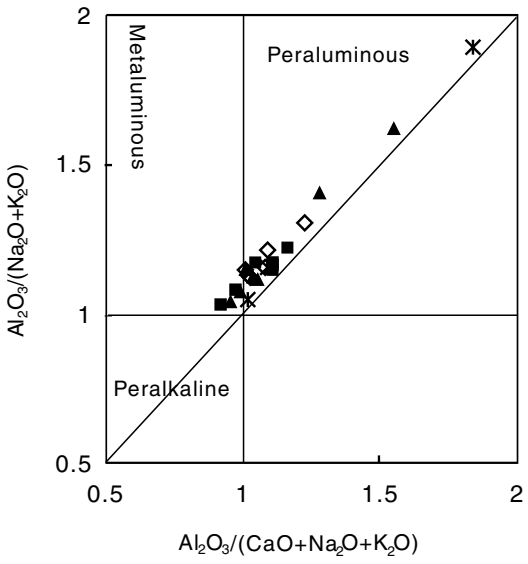

Fig. 5. A plot of $Al_2O_3/(K_2O + Na_2O)$ vs. $Al_2O_3/(CaO + K_2O + Na_2O)$ for granites and rhyolites. (■) red medium-grained granite; (◇) gray medium- to fine-grained granite; (▲) gray fine-grained granite; (∗) rhyolite.

A-type granites are presented for comparison from the Lachlan Fold Belt of Australia (King et al., 1997), Proterozoic Damara Belt of Namibia (Jung et al., 1998), and Eastern China (Qiu et al., 2000; Wu et al., 2002; Bao and Zhao, 2003). The peraluminous A-type granites in Fugang, Guangdong Province, and coastal area of Fujian Province, China, also have low LREE and some HFS contents relative to most A-type granites (Qiu et al., 2000; Bao and Zhao, 2003).

5.2. Tectonic setting and generation

A-type granites can form in both post-orogenic and anorogenic settings (Whalen et al., 1987, 1996; Eby, 1990, 1992; Nedelec et al., 1995). However, it is not easy to distinguish these two settings of A-type granites since they do not have distinctive petrological, mineralogical or geochemical features. Eby (1992) subdivided A-type granites into A1 and A2 groups. The A1 group represent differentiates of mantle-derived magmas like oceanic-island basalts, but were emplaced in a continental rift or intraplate setting. The A2 group represents magmas derived from continental crust

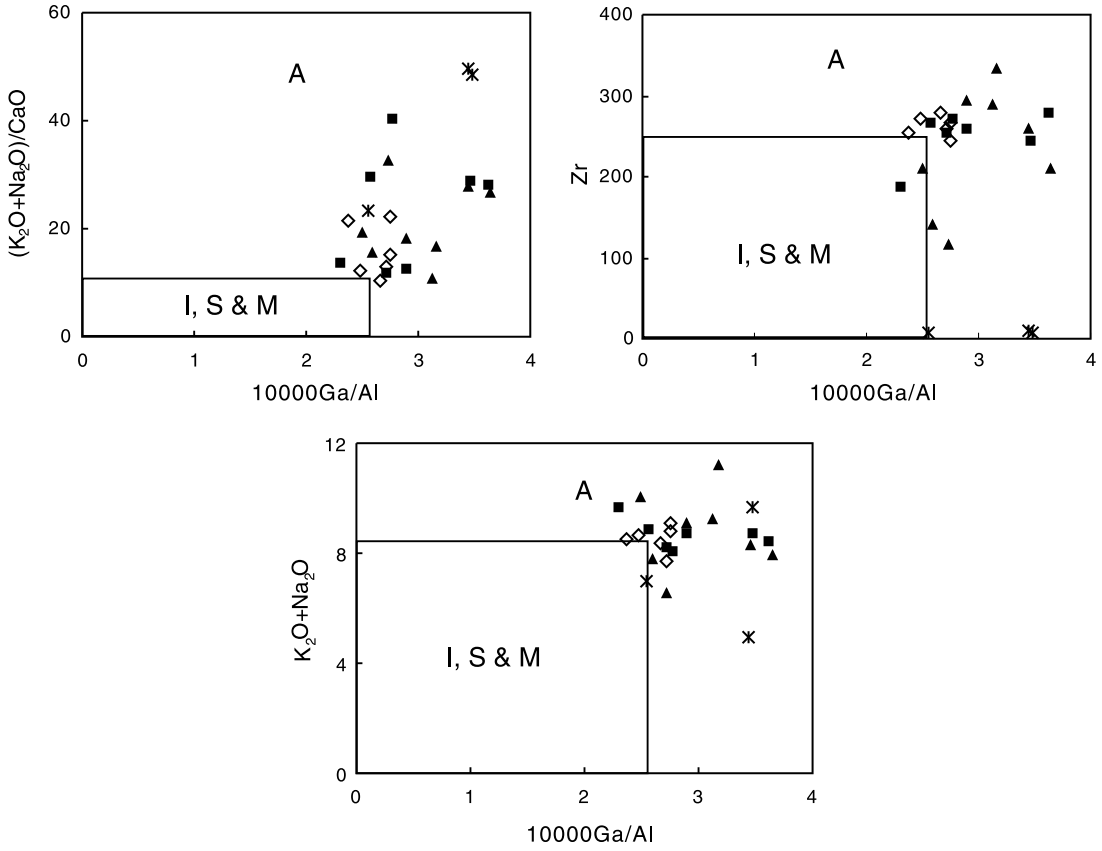

Fig. 6. $(K_2O + Na_2O)/CaO$, Zr and $K_2O + Na_2O$ vs. 10,000Ga/Al discrimination diagrams of Whalen et al. (1987). Symbols same as in Fig. 5.

or underplated crust that have gone through a cycle of continent–continent collision or island-arc magmatism. Using the Ce/Nb–Y/Nb geochemical discriminant diagram of Eby (1992), most of them fall into the A2 group (Fig. 7). In the discrimination diagram (Rb vs. Y + Nb; Fig. 8) of Pearce et al. (1984, 1996), the granites and rhyolites fall in the field of post-collisional granites. By contrast, the Triassic Taihe granites in the Panxi region plot in the within-plate granite (WPG) field (Fig. 8). In the ocean ridge granite-normalized diagram, these granites are characterized by large negative Ba anomalies and enrichment in Ta, Ce, Hf, Zr, Sm, Y, Yb, similar to the within-plate granites (Fig. 9).

During the late Triassic, the Yangtze Block collided with North China, and then, from east to west, with the eastern margin of the Tibetan Plateau (Li et al., 1993; Zhou et al., 2002). In the Danba area of the eastern margin of the

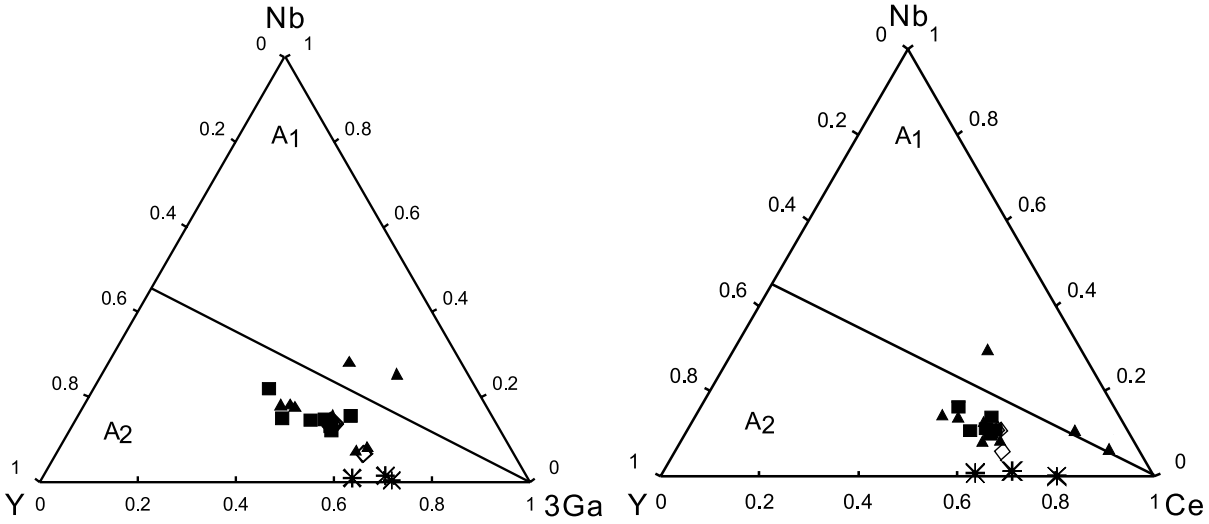

Fig. 7. The A1 and A2 subgroup discriminations of A-type granites after Eby (1992). Symbols same as in Fig. 5.

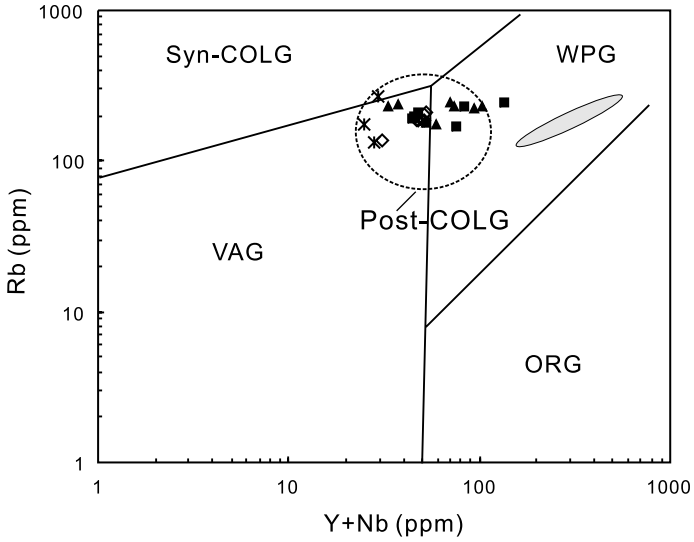

Fig. 8. Rb – (Y + Nb) discrimination diagram after Pearce et al. (1984) and Pearce (1996). VAG, volcanic arc granites; ORG, ocean ridge granites; WPG, within-plate granites; syn-COLG and post-COLG, syn- and post-collisional granites, respectively. The shaded field encompass Taihe granites from the Panxi region (Liu et al., 1988). Symbols same as in Fig. 5.

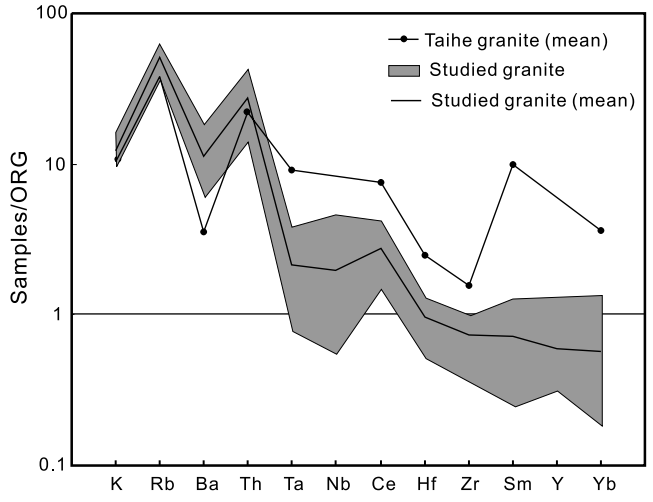

Fig. 9. Ocean ridge granite (ORG)-normalized spidergram for granites. Data sources: ORG from Pearce et al. (1984); Taihe granites from Liu et al. (1988).

Tibetan Plateau, adjacent to the Panxi region, several metamorphic and plutonic domes formed. These are interpreted to be metamorphic core complexes with re-exposure of the western margin of the Yangtze Block that was once subducted underneath the eastern margin of the Tibetan Plateau (Zhou et al., 2002). Zhou et al. (2002) obtained an apparently concordant U–Pb age of 177 Ma on the rim of an oscillatory-zoned zircon from the complex in the Danba area. This age represents the time of metamorphic overgrowth during amphibolith facies metamorphism prior to the exhumation of the block. Thus, the Cretaceous Mianning magmatism clearly post-dated compression and more likely occurred in an extensional environment. Li (2000) subdivided the Yanshanian granitoid magmatism in southeastern China into two phases, i.e., the early (Jurassic) and late (Cretaceous) magmatism. The former was considered to be related to subduction or collision (Campbell and Sewel, 1997), and the later formed within a lithospheric extensional setting (Li, 2000). This shows that the cessation of compression and initiation of a Cretaceous extensional environment in southeastern China (Li, 2000). Wu et al. (2002) also proposed that the Cretaceous A-type granites in northeastern China were related to extension following lithospheric delamination associated with subduction of the Pacific plate. Hence, the lithospheric extension was possibly prevalent in the Cretaceous.

Several petrogenetic models have been proposed for the origin of A-type granites, including (1) fractionation of mantle-derived magmas with or without interaction with crustal rocks (Loiselle and Wones, 1979; Eby, 1990; Foland and Allen, 1991; Turner et al., 1992; Kerr and Fryer, 1993; Anderson et al., 2003); (2) low degrees of partial melting of lower-crustal granulites that were depleted in incompatible elements by previous melt extraction (Collins et al., 1982; Clemens et al., 1986; Whalen et al., 1987); (3) anatexis of undepleted, I-type tonalitic crustal sources (Anderson, 1983; Sylvester, 1989; Creaser et al., 1991; Skjerlie and Johnston, 1992; Patino, 1997); (4) melting of lower-crustal source rocks during fluxing of mantle-derived volatiles or metasomatism of granitic magmas (Taylor et al., 1980; Harris et al., 1986). Evidently, not a single model is suitable for all A-type granitoids. The high initial Sr isotopic ratios (>0.72) and A2 chemical characteristics (Fig. 7) of the Mianning granites are indicative of a clear crustal imprint.

King et al. (1997) suggested that peraluminous A-type granites resulted from parting melting of felsic crustal rocks. However, the peraluminous A-type granites and rhyolites studied here are chemically distinct from those described from the Lachlan Fold Belt (LFB) and Proterozoic Damara Belt (PDB; King et al., 1997; Jung et al., 1998) in having lower TiO_2, CaO, Eu, Sr, Zr, Ni, and Cu contents (Fig. 10). Notably there is no relationship between

($K_2O + Na_2O$) and SiO_2, while the plot of TiO_2 vs. SiO_2 shows a negative trend (Fig. 10). Significant degrees of fractional crystallization have occurred during formation of the granites. This is clearly indicated by negative anomalies in Ba, Sr, P, Ti, and Eu in the spidergrams (Fig. 2) and REE patterns (Fig. 3). Negative Ti anomalies are commonly related to ilmenite or titanite fractionation, whereas a negative P anomaly is attributed to apatite removal. Large negative Eu depletion requires extensive fractionation of feldspars. The Rb, Sr, and Ba variations are useful in estimating whether magmatic evolution was controlled dominantly by fractional crystallization or partial melting (Hanson, 1978, 1989). Plagioclase fractionation would produce negative Sr and Eu anomalies. However, Eu depleFig. 10. $K_2O + Na_2O$ (A), CaO (B), and TiO_2 (C) vs. SiO_2. Other plots include Zr vs. Sr (D), Eu vs. CNK (E), and Cu vs. Ni (F). Diagrams are for granites and rhyolites. LFB, granites from Lachlan Fold Belt of SE Australia (King et al., 1997); PDB, granites from Proterozoic Damara Belt of Namibia (Jung et al., 1998). Symbols same as in Fig. 5.

tion could also be produced by potassium feldspar fractionation, which would explain the negative Ba anomaly. Plots of Eu anomalies versus Ba, and Sr versus Ba correlate positively (Fig. 11), indicating that fractional crystallization was more important than partial melting. Moreover, fractionation of potassium feldspar probably caused an increase in Rb and decreases in both Sr and Ba, accompanied by a decrease in K/Rb ratios (Fig. 11).

In order to test the fractional crystallization process, Rb and Sr are plotted in a log–log diagram (Fig. 12). We selected Sr because this element is not significantly accommodated in accessory minerals (e.g., oxides, zircon; Ewart and Griffin, 1994). For comparison, the equations for batch partial melting (a; Schilling and Winchester, 1967) and Rayleigh fractionation crystallization (b; Neumann et al., 1954) are used, respectively:

$$C_L^i = \frac{C_0^i}{D + F(1-D)} \quad \text{(a)}$$

in which C_L and C_0 are the concentrations of element i in the derivative partial melt and in the protolith, respectively, while F is the fractional proportion of melt formed. D is the bulk distribution coefficient of trace element i between the melt and residue at the time of melt separation from the residue: $D = \sum_j X_j K_d^{j/\text{melt}}$. X_j is the weight fraction of mineral j in the restite and K_d is the partition coefficient for element i between the mineral j and the melt.

$$\frac{C_L^i}{C_0^i} = F^{(D-1)} \quad \text{(b)}$$

where C_L and C_0 are the concentrations of element i in the differentiated melt and in the parent melt, respectively. F is the fraction of melt remaining and D is the bulk distribution coefficient for the element relative to the crystallizing assemblage.

We have taken the Rb and Sr contents of the protolith or parent melt (Rb = 79 ppm and Sr = 254 ppm) from data on the total crust of the Yangtze Block (Gao et al., 1998). The X_j ($X_{\text{plagioclase}} = 0.5$ and $X_{\text{cpx}} = 0.5$ ignoring minor minerals like oxides) and partition coefficients are estimated from Rapp and Watson (1995) and Bacon and Druitt (1988), respectively. With these parameters, we get $D_{\text{Rb}} = 0.16$ and $D_{\text{Sr}} = 2$. The Rb–Sr trend of the granites is not adequately reproduced by batch partial melting

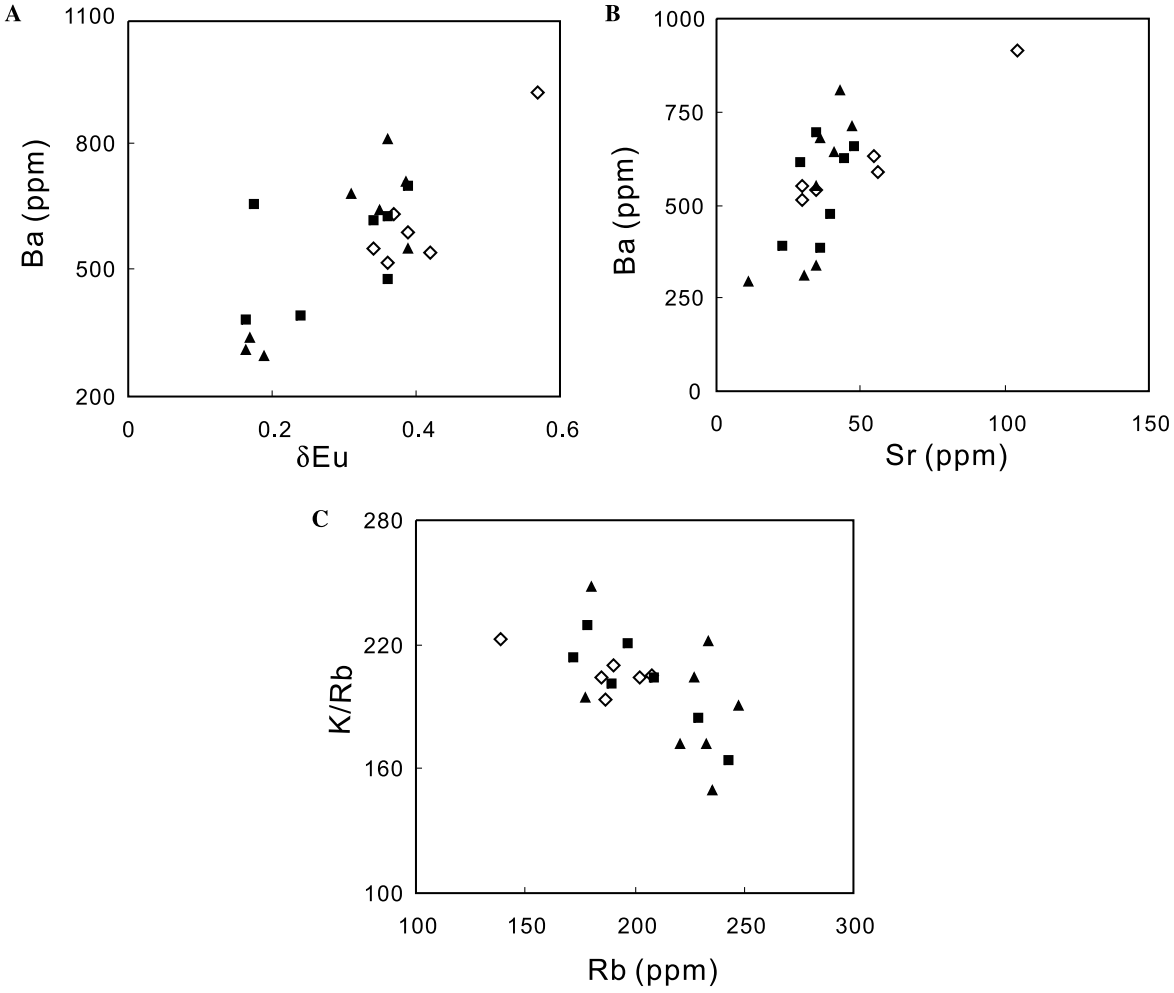

Fig. 11. Ba vs. δEu (A), Ba vs. Sr (B), and K/Rb vs. Rb (C) plots for granites. Symbols same as in Fig. 5.

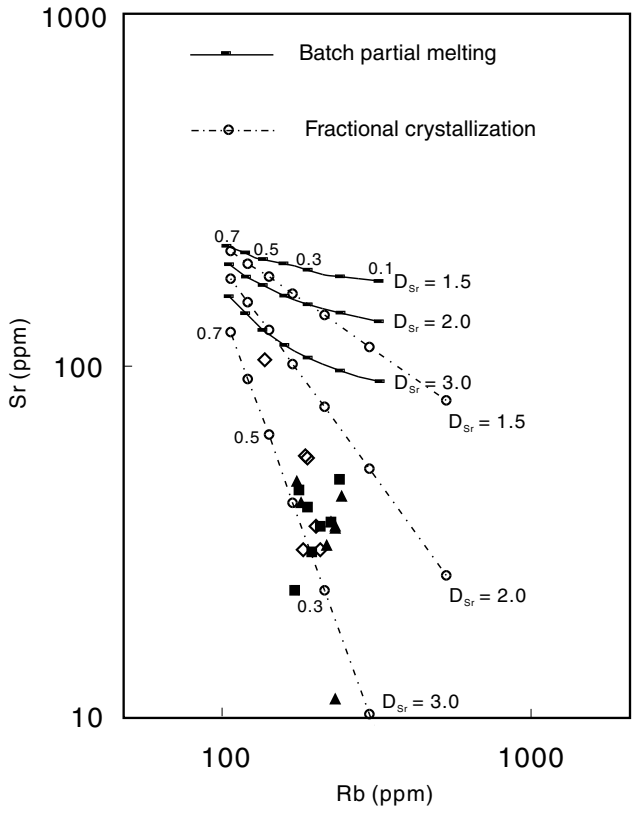

Fig. 12. Sr vs. Rb diagram. Curves show the batch partial melting and fractional crystallization models for three different D_{Sr}. Numbers along curves refer to the degree of partial melting and the degree of crystallization. Symbols same as in Fig. 5.

(Fig. 12), even by varying D_{Sr} (between 3 and 1.5). In contrast, fractional crystallization modeling shows a better fit.

It has been shown that many of these samples are highly fractionated, which means their Rb/Sr ratios are probably considerably greater than that of the primary magma. High Rb/Sr makes calculating an accurate initial $^{87}Sr/^{86}Sr$ ratio difficult. The calculated initial Sr isotopic ratios yield high and variable results. This is in contrast to Sm–Nd isotopic results, which yield a small range of moderately negative ε_{Nd} (−1.5 to −3.2) values and young Depleted Mantle model ages ranging from 630 to 1030 Ma (Table 2).

5.3. Metallogenic implications

The Panxi region is a typical, well-developed continental rift. Rifting started in the early Paleozoic, developed in the late Paleozoic, and terminated during the Indosinian epoch (Cong, 1988; Zhang et al., 1988). Many deposits formed during this period, including Cu–Ni, Pt, Fe–Ti–V, Nb–Ta–Zr–Hf deposits. During the Cenozoic, the rift was reactivated due to the Himalayan orogeny that resulted in uplift of the Tibetan Plateau. A large REE deposit, hosted in a carbonatite–syenite complex, formed in Maoniuping (Fig. 1). The Devonian gabbros and Paleogene syenite–carbonatite complex in this area have low initial Sr isotopes (0.7034–0.7054, 0.7060–0.7063, respectively; Zhang et al., 1988; Xu et al., 2003b). The initial $^{87}Sr/^{86}Sr$ ratio of the Triassic granites is 0.7089, based on the regression of whole-rock Rb–Sr data (Yuan et al., 1985). The Cretaceous granites show high initial $^{87}Sr/^{86}Sr$ values (>0.72). It is obvious that mantle activity had been weakened in the late Mesozoic based on the high Sr isotopes, even though this was a time of significant mineralization in southeastern China (Hua and Mao, 1999; Mao and Hua, 1999). Studies show that although the granitoids of southeastern China are dominated by recycled continental crust, the mantle component played an important part in the generation of Cretaceous granitoids in southeastern China (Jahn et al., 1990, 2000; Chen and Jahn, 1998; Li, 2000). Hua et al. (2003) suggested that the late Mesozoic metallogenic processes related to granitoids were the result of mantle–crust interactions in southeastern China. It was the active involvement of mantle material that resulted in large-scale magmatic activity, and promoted large-scale mineralization in that area. Thus, the weakening of mantle activity was a main factor that resulted in the waning of late Mesozoic metallogenesis in the Panxi region.

6. Conclusions

The following conclusions can be drawn from this work:

1. The Cretaceous granites from Mianning in the Panxi region are peraluminous to slightly metaluminous and are A-type.
2. The rocks formed in a post-collisional setting subsequent to collision of the Tibetan Plateau and Yangtze Block and were generated by crystal fractionation from a crustal source. In the late Mesozoic, the dominance of a crustal component over mantle material resulted in diminished metallogenic activity in the Panxi region.

Acknowledgements

We thank Prof. J. Lawford Anderson of the University of Southern California, Prof. Bor-ming Jahn of National Taiwan University and one anonymous reviewer for reviewing and improving the manuscript. We are grateful to Dr. Charlotte Allen of the Australian National University for revising the manuscript and good suggestion. This work was financially supported by Chinese Natural Science Foundation Grant No. 40303004.

References

Anderson, J.L., 1983. Proterozoic anorogenic granite plutonism of North America. Geological Society of America, Memoir 161, 133–154.

Anderson, J.L., Morrison, J., 1992. The role of anorogenic granites in the Proterozoic crustal development of North America. Developments in Precambrian Geology 10, 263–299.

Anderson, I.C., Frost, C.D., Frost, B.R., 2003. Petrogenesis of the Red Mountain pluton, Laramie anorthosite complex, Wyoming: implica-

tions for the origin of A-type granite. Precambrian Research 124, 243–267.

Bacon, C.R., Druitt, T.H., 1988. Compositional evolution of the zoned calcalkaline magma chamber of Mount Mazama, Crater Lake, Oregon. Contributions to Mineralogy and Petrology 98, 145–153.

Bao, Z.W., Zhao, Z.H., 2003. Geochemistry and tectonic setting of the Fugang aluminous A-type granite, Guangdong Province, China: a preliminary study. Geology-Geochemistry 31, 52–61 (in Chinese with English abstract).

Boynton, W.V., 1984. Cosmochemistry of the rare earth elements: meteorite studies. In: Handerson, P. (Ed.), Rare Earth Geochemistry. Elsevier, Amsterdam, pp. 63–114.

Campbell, S.D.G., Sewel, R.J., 1997. Structure control and tectonic setting of Mesozoic volcanism in Hong Kong. Journal of the Geological Society of London 154, 1039–1052.

Chen, B., Jahn, B.M., 1998. Crustal evolution of southeastern China: Nd and Sr isotopic evidence. Tectonophysics 284, 101–133.

Clemens, J.D., Holloway, J.R., White, A.J.R., 1986. Origin of an A-type granite: experimental constraints. American Mineralogist 71, 317–324.

Collins, W.J., Beams, S.D., White, A.J.R., Chappel, B.W., 1982. Nature and origin of A-type granites with particular reference to southeastern Australia. Contributions to Mineralogy and Petrology 80, 189–200.

Cong, B.L., 1988. The Formation and Evolvement of Panxi Paleorift. Science Press, Beijing (in Chinese).

Creaser, R.A., Price, R.C., Wormald, R.J., 1991. A-type granites revisited: assessment of a residual-source model. Geology 19, 163–166.

Deniel, C., Vidal, P.H., Fernandez, A., LeFort, P., Peucat, J.J., 1987. Isotopic study of the Manaslu granite (Himalay Nepal). Contributions to Mineralogy and Petrology 86, 78–92.

DePaolo, D.J., 1981. Neodymium isotopes in the Colorado Front Range and crust–mantle evolution in the Proterozoic. Nature 291, 193–196.

Eby, G.N., 1990. The A-type granitoids: a review of their occurrence and chemical characteristics and speculations on their petrogenesis. Lithos 26, 115–134.

Eby, G.N., 1992. Chemical subdivision of the A-type granitoids: petrogenetic and tectonic implications. Geology 20, 641–644.

Ewart, A., Griffin, W.L., 1994. Application of proton-microprobe data to trace element partitioning in volcanic rocks. Chemical Geology 117, 251–284.

Foland, K.A., Allen, J.C., 1991. Magma sources for Mesozoic anorogenic granites of the White Mountain magma series, New England, USA. Contributions to Mineralogy and Petrology 109, 195–211.

Gao, S., Luo, T.C., Zhang, B.R., Zhang, H.F., Han, Y.W., Zhao, Z.D., Hu, Y.K., 1998. Chemical composition of the continental crust as revealed by studies in east China. Geochimica et Cosmochimica Acta 62, 1959–1975.

Hanson, G.N., 1978. The application of trace elements to the petrogenesis of igneous rocks of granitic composition. Earth and Planetary Science Letters 38, 26–43.

Hanson, G.N., 1989. An approach to trace element modeling using a simple igneous system as an example. In: lipin, B.R., McKay, G.A. (Eds.), Geochemistry of Mineralogy of Rare Earth Elements, Review in Mineralogy 21, 79–97.

Harris, N.B.W., Marzouki, F.M.H., Ali, S., 1986. The Jabel Sayid complex, Arabian shield: geochemical constraints on the origin of peralkaline and related granites. Journal of Geological Society, London 143, 287–295.

Hua, R.M., Mao, J.W., 1999. A preliminary discussion on the Mesozoic explosion in East China. Mineral Deposits 18, 300–308 (in Chinese with English abstract).

Hua, R.M., Chen, P.R., Zhang, W.L., Liu, X.D., Lu, J.J., Lin, J.F., Yao, J.M., Qi, H.W., Zhang, Z.S., Gu, S.Y., 2003. Metallogenic systems related to Mesozoic and Cenozoic granitoid in south China. Science in China (D) 46, 816–829.

Inger, S., Harris, N., 1993. Geochemical constraints on leucogranite magmatic in the Langtang Valley, Nepal Himalaya. Journal of Petrology 34, 345–368.

Jahn, B.M., Zhou, X.H., Li, J.L., 1990. Formation and tectonic evolution of southeastern China and Taiwan: isotopic and geochemical constrains. Tectonophysics 183, 145–160.

Jahn, B.M., Wu, F.Y., Chen, B., 2000. Massive granitoid generation in Central Asia: Nd isotope evidence and implication for continental growth in the Phanerozoic. Episode 23, 82–92.

Jung, S., Mezger, K., Hoernes, S., 1998. Petrology and geochemistry of Syn- to post-collisional metaluminous A-type granites – a major and trace element and Nd–Sr–Pb–O-isotope study from the proterozoic Damara Belt, Namibia. Lithos 45, 147–175.

Kerr, A., Fryer, B.J., 1993. Nd isotope evidence for crust–mantle interaction in the generation of A-type granitoid suites in Labrador, Canada. Chemical Geology 104, 39–60.

King, P.L., White, A.J.R., Chappell, B.W., Allen, C.M., 1997. Characterization and origin of aluminous A-type granites from the Lachlan Fold Belt, southeastern Australia. Journal of Petrology 38, 371–391.

Li, X.H., 2000. Cretaceous magmatism and lithospheric extension in the Southeast China. Journal of Asian Earth Sciences 18, 293–305.

Li, S.G., Xiao, Y.L., Liou, D.L., Chen, Y.Z., Ge, N.J., Zhang, Z.Q., Sun, S.S., Cong, B.L., Zhang, R.Y., Hart, S.R., Wang, S.S., 1993. Collision of the North china and Yangtze blocks and formation of coesite-bearing eclogites: timing and processes. Chemical Geology 109, 89–111.

Liu, Y.R., Jin, M.X., Xing, X.F., Shen, G.F., 1988. Granitoids and Their Metallogenetic Characteristics in Xichang-Middle Part of Yunnan. Chongqing Publishing House, Chongqing (in Chinese).

Loiselle, M.C., Wones, D.R., 1979. Characteristics and origin of anorogenic granites. Geological Society of America 11, 468 (Abstract with Programs).

Maniar, P.D., Piccoli, P.M., 1989. Tectonic discrimination of granitoids. Geological Society of America Bulletin 101, 635–643.

Mao, J.W., Hua, R.M., 1999. A preliminary study of large-scale metallogenesis and large clusters of mineral deposits. Mineral Deposits 18, 291–299 (in Chinese with English abstract).

Nedelec, A., Stephens, W.E., Fallick, A.E., 1995. The Panafrican stratoid granites of Madagascar: alkaline magmatism in a post-collisional extensional setting. Journal of Petrology 36, 1367–1391.

Neumann, H., Mead, J., Vitaliano, C.J., 1954. Trace element variations and during fractional crystallization as calculated from the distribution law. Geochimica et Cosmochimica Acta 6, 90–99.

Niu, H.C., 1994. REE mineralization related to syenites. Guangzhou Institute of Geochemistry, Chinese Academy of Sciences, Postdoctoral Report.

Patino, D.A.E., 1997. Generation of metaluminous A-type granites by low-pressure melting of calc-alkaline granitoids. Geology 25, 743–746.

Pearce, J.A., 1996. Sources and settings of granitic rocks. Episodes 19, 120–125.

Pearce, J.A., Harris, N.B.W., Tindle, A.G., 1984. Trace element discrimination diagrams for the Tectonic interpretation of granitic rocks. Journal of Petrology 25, 956–983.

Pu, G.P., 2001. The evolution history of REE mineralization and major features of Himalayan REE deposit in Panzhihua-Xichang area, Sichuan. In: Chen, Y.C., Wang, D.H. (Eds.), Study on Himalayan Endognic Mineralization. Geological Publishing House, Beijing, pp. 104–116 (in Chinese).

Qi, L., Hu, J., Gregoire, D.C., 2000. Determination of trace elements in granite by inductively coupled plasma mass spectrometry. Talanta 51, 507–513.

Qiu, J.S., Wang, D.Z., Satoshi, K., McInnes, B.I.A., 2000. Geochemistry and petrogenesis of aluminous A-type granites in the coastal area of Fujian Province. Geochimca 29, 313–321 (in Chinese with English abstract).

Rapp, R.P., Watson, E.B., 1995. Dehydration melting of metabasalt at 8–32 kbar: implications for continental growth and crust–mantle recycling. Journal of Petrology 36, 891–931.

Schilling, J.G., Winchester, J.W., 1967. Rare earth fractionation and magmatic processes. In: Runcorn, S.K. (Ed.), Mantle of Earth and Terrestrial Planets. Interscience, London, pp. 267–283.

Skjerlie, K.P., Johnston, A.D., 1992. Vapor-absent melting at 10 kbar of a biotite- and amphibole-bearing tonalitic gneiss: implications for the generation of A-type granites. Geology 20, 263–266.

Sun, S.-S., McDonough, W.F., 1989. Chemical and isotopic systematics of oceanic basalt: implications for mantle compositions and processes. In: Saunders, A.D., Norry, M.J. (Eds.), Magmatism in the Ocean Basins. Geological Society of Special Publish 42, 313–345.

Sylvester, P.J., 1989. Post-collisional alkaline granites. Journal of Geology 97, 261–281.

Taylor, R.P., Strong, D.F., Kean, B.F., 1980. The Topsails igneous complex: Silurian-Devonian peralkaline magmatism in western Newfoundland. Canadian Journal of Earth Science 17, 425–439.

Turner, S.P., Foden, J.D., Morrison, R.S., 1992. Derivation of some A-type magmas by fractionation of basaltic magma: an example from the Padthaway ridge, South Australia. Lithos 28, 151–179.

Whalen, J.B., Currie, K.L., Chappell, B.W., 1987. A-type granites: geochemical characteristics, distribution and petrogenesis. Contributions to Mineralogy and Petrology 95, 407–419.

Whalen, J.B., Jenner, G.A., Longstaffe, F.J., Robert, F., Gariepy, C., 1996. Geochemical and isotopic (O, Nd, Pb and Sr) constraints on A-type granite: petrogenesis based on the Topsails igneous suits, Newfoundland Appalachians. Journal of Petrology 37, 1463–1489.

Wu, F.Y., Sun, D.Y., Li, H., Jahn, B.M., Wilde, S., 2002. A-type granites in northeastern China: age and geochemical constraints on their petrogenesis. Chemical Geology 187, 143–173.

Xu, C., Huang, Z.L., Liu, C.Q., Qi, L., Li, W.B., Guan, T., 2003a. Sources of ore-forming fluids in the Maoniuping REE deposit, Sichuan Province, China- evidence from REE, radiogenic Sr, Nd, and stable isotopes. International Geology Review 45, 635–645.

Xu, C., Huang, Z.L., Liu, C.Q., Qi, L., Li, W.B., Guan, T., 2003b. Geochemistry of carbonatites in Maoniuping REE deposit Sichuan Province, China. Science in China (D) 46, 246–256.

Yuan, H.H., Zhang, S.F., Zhang, P., 1985. Isotopic chronologic study of magmatites in Panxi rift. In: Zhang, Y.X., Liu, B.G. (Eds.), Proceedings of Symposium on Panxi Rift in China (1). Geological Publishing House, Beijing, pp. 241–257 (in Chinese).

Zhang, Y.X., Lu, Y.N., Yang, C.X., 1988. The Panxi Rift. Geological Publishing House, Beijing (in Chinese).

Zhang, H.F., Harris, N., Parrish, R., Zhang, L., Zhao, Z.D., Li, D.W., 2005. Geochemistry of North Himalayan leucogranites: regional comparison, petrogenesis and tectonic implications. Earth Science 30, 275–288 (in Chinese with English abstract).

Zhou, M.F., Yan, D.P., Kennedy, A.K., Li, Y., Ding, J., 2002. SHRIMP U–Pb zircon geochronological and geochemical evidence for Neoproterozoic arc-magmatism along the western margin of the Yangtze Block, South China. Earth and Planetary Science Letters 196, 51–67.